Density of states in a single PbSe/PbS core-shell quantum dot measured by scanning tunneling spectroscopy

G. A. Grinbom,[1,2] M. Saraf,[1,2,*] C. Saguy,[2] A. C. Bartnik,[3] F. Wise,[3] and E. Lifshitz[1,2,†]
[1]*Schulich Faculty of Chemistry, Russell Berrie Nanotechnology Institute, Technion, Haifa 32000, Israel*
[2]*Solid State Institute, Technion, Haifa 32000, Israel*
[3]*Applied Physics Department, Cornell University, Ithaca, New York 14853, USA*
(Received 1 December 2009; revised manuscript received 25 March 2010; published 1 June 2010)

The electronic configuration of a set of PbSe/PbS core-shell colloidal quantum dots (CQDs), with a common core radius of 1.5 nm having a PbS shell of a variable width from 0.75 to 2.5 nm, was investigated by scanning tunneling spectroscopy. The conductance resonance spectra were correlated with a band tunneling process, monitoring the individual electronic levels of conduction and valence bands. The energy band gap of the various samples, derived from the conductance spectra, were compared with the values measured by the absorption spectra, as well as with a theoretical evaluation, using the extended four-band envelope function theory across the PbSe/PbS material boundary. The experimental results showed a decrease in the energy band gap, as well as a decrease in a few higher energy interband transitions, with the increase in the shell thickness, in close agreement with the theoretical prediction, which correlated it with a delocalization of the carriers' wave functions over the entire core-shell structure. However, the increase in the outer radius of the core-shell CQDs has a slightly smaller influence than a simple growth in size of PbSe cores, due to the existence of Fermi-energy offset, discontinuity in the effective mass and the dielectric constant at the core-shell interface.

DOI: 10.1103/PhysRevB.81.245301 PACS number(s): 73.22.−f, 73.21.La, 73.63.Kv, 68.37.Ef

I. INTRODUCTION

PbS and PbSe colloidal quantum dots (CQDs) are the focus of vast interest due to their unique electronic and optical properties,[1–3] with feasibility in a variety of optoelectronic applications in the near infrared (NIR) region, including gain devices,[2] optical switches,[4] photovoltaic cells,[5–8] and biological labeling.[9,10] The bulk PbS and PbSe semiconductors have a rock-salt crystal structure with nearly identical lattice constants (5.93 Å and 6.12 Å at 300 K, respectively), facilitating the formation of heterostructures. Furthermore, the bulk IV-VI semiconductors have a narrow direct band gap ($E_{g(PbSe)}=0.28$ eV and $E_{g(PbS)}=0.4$ eV at 300 K) with both valence and conduction band edges being fourfold degenerated at the L point of the Brillouin zone (eightfold when including spin degeneracy). Also, these semiconductors have relatively large optical ($\varepsilon_{\infty}=18.0-24.0$) and static ($\varepsilon_{s(PbSe)}=227$ and $\varepsilon_{s(PbS)}=161$) dielectric constants, small effective masses of electron and hole ($m_{e,h}\leq 0.1m_0$), and a large effective Bohr radii ($a_{B(PbSe)}=46$ nm and $a_{B(PbS)}=18$ nm).

The colloidal synthesis of PbSe CQDs, in organic or water solutions, has been developed in the past decade.[11] Brumer *et al.*[12] produced high-quality PbSe/PbS core-shell CQDs and completely original PbSe/PbSe$_x$S$_{1-x}$ core-alloyed shell CQDs. Another recent report[13] showed the formation of PbSe/CdSe/ZnSe core-shell CQDs. The core-shell structures of the IV-VI semiconductors exhibit close crystallographic matching at the core-shell interface, chemical robustness at ambient conditions over a length of time (months and years)[2] and high photoluminescence quantum yield (45% in PbSe/PbS and >70% in PbSe/PbSe$_x$S$_{1-x}$ CQDs).[12] These structures also offer tunability of the energy band gap with the change in the Se/S composition and the core-radius/shell-width ratio (*vide infra*).[2] In particular, the PbSe/PbSe$_x$S$_{1-x}$ core-alloyed shell CQDs demonstrate a gradual change in the Se/S ratio, when moving from the interior core-shell interface toward the shell exterior surface. This gradual transfer minimizes the occurrence of trapping sites and avoids discontinuity in the dielectric constant at the core-shell interface.[4,12] Moreover, the Auger relaxation process and fluorescence blinking, which have been topics of major concern in recent years,[14] could be partially suppressed in samples with a better crystallographic and dielectric matching between a core and its surrounding, and when partial carriers' separation between the core and the shell takes place (*vide infra*).[15] Such conditions should reduce existing many-body (if generated) Coulomb interactions within a CQD and provide a substantial benefit in solar-energy applications and gain devices.

The electronic structure of IV-VI core CQDs still remains a matter of controversy and even less is known about the properties of the core-shell structures. Calculations within the framework of the effective-mass approximation revealed that conduction and valence bands of core CQDs are nearly symmetric.[1] The tight-binding and the atomistic pseudopotential calculations[3,16–18] of PbSe revealed an L-point intervalley coupling and anisotropy of effective masses. It was also suggested that the adjacent Σ and K Brillouin zone extremes could lift the degeneracy of the electronic levels.[16]

Bartnik *et al.*[19] presented a theoretical description (the only one currently offered) of the electronic structure of PbSe/PbS core-shell CQDs, using the extended four-band envelope function theory across the PbSe/PbS material boundary. Their study found two types of behavior: (a) CQDs with an outer radius of 1.5–5 nm experience an extension of both electron and hole wave functions over the entire structure with an increase in the delocalization with the increase in the core-shell total size (type I); (b) CQDs with an outer radius ≥7 nm are influenced by the core-shell barrier, when the lowest unoccupied molecular orbital (LUMO) is localized in

the core while the highest occupied molecular orbital (HOMO) is delocalized, with a larger weight within the shell on the increase in the shell width (type II), similar to the expectation derived from the corresponding bulk semiconductor.[20] Thus, the electronic structure of PbSe/PbS core-shell CQDs depends on the outer radius, as well as on the core-radius/shell-width ratio.

While a theoretical model predicts the electronic configuration of the IV-VI core-shell CQDs, the existing experimental evidence is not sufficient. The optical absorbance, continuous wave, and time-resolved photoluminescence (PL) and PL-excitation spectra have been explored in recent years,[2,21,22] but these optical methods basically detect transitions between two states, yet leave a debate regarding the electronic nature of core-shell structures. Overcoming this limitation, the current study used scanning tunneling spectroscopy (STS), monitoring separately the density of states of the valence and conduction bands. STS has been previously applied in the investigation of semiconductor CQDs of CdSe,[23] PbSe,[24] and InAs (Ref. 25) CQDs, InAs rods,[26] as well as in the study of InAs/ZnSe (Ref. 25) and ZnSe/CdSe (Ref. 27) core-shell structures. The current study describes the investigation of a set of PbSe/PbS core-shell CQDs with various core-radius/shell-width ratios, when with a common core radius of 1.5 nm and a variable shell width (w) from 0.75 to 2.5 nm. The results revealed a decrease in the energy band gap with the increase in the shell thickness, changes that were correlated with a delocalization of the carriers' wave functions over the entire core-shell structure, restricted by the Fermi-energy offset, the discontinuity of the effective masses and the dielectric constant at the core-shell interface.[20]

II. EXPERIMENTAL

PbSe cores CQDs, covered with oleic acid surfactants, were prepared according to a procedure given in Ref. 12. PbSe/PbS core-shell CQDs with a shell width up to ~1.8 nm (also capped with oleic acid molecules) were prepared via a single injection of shell constituents of the appropriate stoichiometry amounts at ~130 °C into a freshly prepared (free of Se monomers) PbSe core solution (see Ref. 12). However, core-shell CQDs with a shell thickness >1.8 nm required repeated injections (2–4 times) of the shell elements until the desired thickness was achieved. Representative aliquots were drawn from the reaction solution during the growth and their absorption and transmission electron microscopy (TEM) images were monitored. The absorption spectra were recorded on a spectrometer model UV-VIS-NIR spectrometer JASCO V-570 and the TEM images were recorded using a FEI Tecnai G^2 T20 S-Twin instrument, operating at 200 kV.

The scanning tunneling microscopy (STM) and the STS measurements of a single-core or core-shell CQD were done by depositing CQDs onto a gold [Au(111)] thin film, supported on a Mica substrate, and treated with a self-assembled hexanedithiol monolayer. This self-assembled monolayer was prepared by immersing the gold films overnight in a solution, while any noncovalently linked thiol molecules were rinsed away from the surface. Then uniform and isolated CQDs coverage was formed by immersing thiol-treated gold films in a chloroform solution suspended with a low concentration of CQDs for a limited duration (1 min). Thus, isolated CQDs were anchored to the gold substrate via thiol linking groups, immobilized by the scanning tip during the experiment. The gold-coated CQDs were further annealed at 110 °C overnight within the STM chamber in ultrahigh vacuum (UHV), removing any excess contamination.

The topography and the electronic structure of a single PbSe/PbS core-shell CQD were measured by the use of a STM/STS Omircon Nanotechnology system (UHV variable temperature scanning probe microscopy), operating at 25 K in UHV (4×10^{-11} mbar) conditions. The STM images were achieved with a bias voltage (V_{bias}) of 2 V and a set-point current of 5–50 pA, adjusting a feedback loop to keep a constant current. The current-voltage (I-V) curves were measured by positioning an atomistic edge tip above a single dot and interrupting the feedback loop. The conductance spectra (dI/dV_{bias} versus V_{bias}) were obtained either by a numerical differentiation of the I-V curves or by a direct measure via a lock-in amplifier. A set-point current up to 70 pA was used when the voltage was altered between −2 V to +2 V. The reproducibility of the data was ensured by recording I-V curves of a single CQD hundreds of times, and the data were smoothed by averaging over various accumulations.

III. RESULTS

This work describes a comparison between the electronic structure of a PbSe core with a radius (r_c) of 1.5 nm and corresponding PbSe/PbS core-shell structures with an outer radii (r_{cs}) of 2.25, 3, and 4 nm. A representative TEM image of core-shell CQDs is shown in Fig. 1(a). The image exhibits a few CQDs, with a distinct appearance of core and shell areas, with a shell width of 1.5 nm, nearly equivalent to the radius of the core. Figure 1(b) compares the absorption spectra of core-shell CQDs with $r_{cs}=2.25$ nm with the spectrum of the corresponding core ($r_c=1.5$ nm) revealing a substantial redshift on the addition of a thin shell ($w=0.75$ nm). Figure 1(c) represents a STM image of PbSe/PbS CQDs dispersed on a gold substrate with $r_{cs}=4$ nm, recorded with a bias voltage of 2 V and a set-point current of 5 pA. The inset shows a height profile of a single CQD shown in the figure, however, the lateral dimensions of the profile are substantially larger than the actual size, due to a broadening of the tip width, thus, the height alone indicates the CQD's diameter. Figure 1(d) shows a typical height histogram of the CQDs examined.

Figure 2 shows conductance spectra, represented as a plot of dI/dV_{bias} versus V_{bias}, of a PbSe core with $r_c=1.5$ nm (bottom curve) and corresponding core-shell CQDs with r_{cs} values of 2.25, 3, and 4 nm (from bottom to top), all recorded with a set-point current of 70 pA. The spectra consist of relatively broad tunneling resonances on both sides of $V_{bias}=0$. The resonances at negative bias relate to the hole levels while those at the positive bias are related to the electron levels. The first resonances from both sides of $V_{bias}=0$ correspond to HOMO and LUMO, respectively. The bias dif-

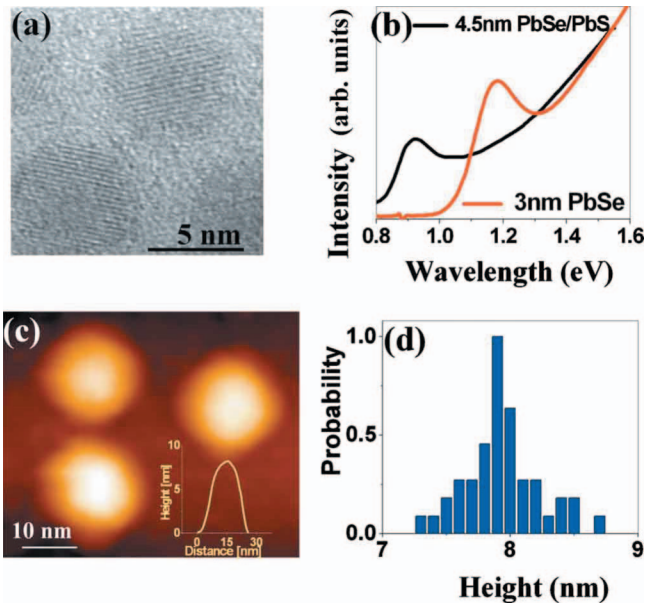

FIG. 1. (Color) (a) A TEM image of PbSe/PbS CQDs with a core radius (r_c) of 1.5 nm and a shell width (w) of 1.5nm. (b) Absorption spectra of PbSe core with r_c=1.5 nm and PbSe/PbS core-shell CQDs with an outer radius (r_{cs}) of 2.25 nm. (c) A STM image of PbSe/PbS CQDs (r_{cs}=4.0 nm) spread over a gold substrate. A height profile of a single CQD is shown in the inset. (d) Typical CQD's height histogram.

ference between them corresponds to the zero-conductance gap. The figure shows that, as expected, this conductance gap is reduced with the increase in the shell width. The discussion in Sec. IV develops the energy band-gap dependence as a function of the outer radius of the PbSe/PbS CQDs and the higher energy interband transitions, based on the given STS and absorption measurements.

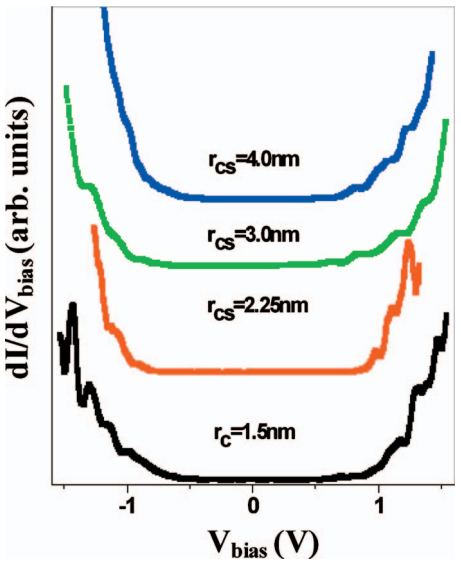

FIG. 2. (Color) Representative conductance spectra, showing a plot of dI/dV_{bias} versus V_{bias}, of a single PbSe core (with a radius r_c), and several PbSe/PbS core-shell CQDs (with an outer radius of r_{cs}).

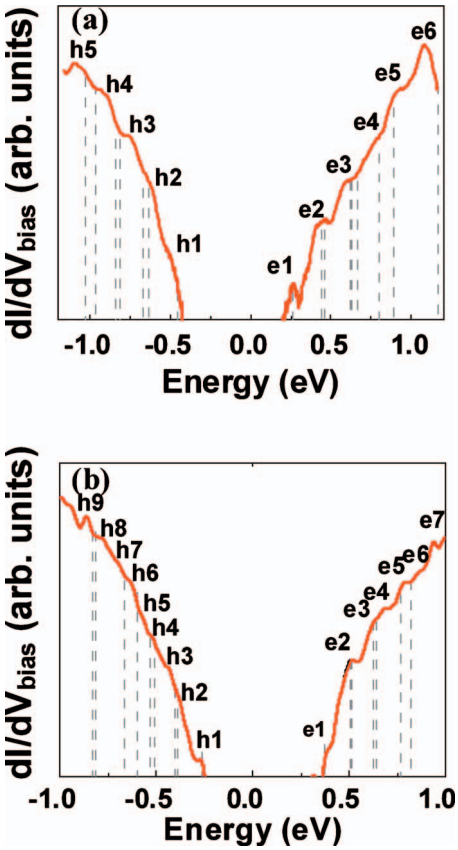

FIG. 3. (Color) Conductance spectra of PbSe/PbS CQDs with core radius of 1.5 nm and an outer radius of (a) 3.0 nm and (b) 4.0 nm, presented as a log plot of dI/dV_{bias} versus E. The grey sticks mark the theoretical intraband energy levels. The (h1, h2,…) and (e1, e2,…) refer to hole and electron-energy levels, respectively.

IV. DISCUSSION

Positioning a single CQD between an atomistic tip and a substrate immediately creates a double-barrier tunnel junction (DBTJ), when the conductance spectrum of a single CQD is related to resonant tunneling of electrons (holes) across the DBTJ. The barriers are located between the CQD and the substrate and between the tip and the CQD. Upon the application of a bias across the tip-CQD-substrate assembly, a voltage drop is created, proportional to the capacitance of tip-dot ($C_{tip\text{-}dot}$) and dot-substrate ($C_{dot\text{-}sub}$) junctions, according to a parameter, η, when[28]

$$\eta = \frac{C_{dot\text{-}sub}}{C_{tip\text{-}dot} + C_{dot\text{-}sub}}. \quad (1)$$

The capacitance values rely on the tip-dot ($d_{tip\text{-}dot}$) and dot-substrate ($d_{dot\text{-}sub}$) surface-to-surface distances, the radius of the CQD (r_c or r_{cs}), the tip radius (r_{tip}=0.5–2.0 nm), and the vacuum dielectric constant, ε_0. The capacitance values are given by the following relations:[28]

$$C_{tip\text{-}dot} = \gamma 2\pi\varepsilon_0 r_{tip}\left[\ln\left(\frac{r_{tip}}{\gamma d_{tip\text{-}dot}}\right) + \ln 2 + \frac{23}{20}\right], \quad (2a)$$

TABLE I. Comparison between the measured (Fig. 3) and the predicted (theory) energy values of valence and conduction electronic levels of PbSe/PbS core-shell CQDs with r_{cs}=3 and 4 nm. The electronic assignments are given at the right column.

r_{cs}						
	3 nm			4 nm		
Label	STS (eV)	Theory (eV)	Label	STS (eV)	Theory (eV)	$(\pi)(n)(l)$
e1	0.26	0.26	e1	0.39	0.37	−1S
e2	0.45	0.45	e2	0.53	0.51	+1P
		0.46			0.52	+1S
e3	0.59	0.62	e3	0.63	0.63	−1D
		0.63	e4	0.69	0.64	−1P
		0.67			0.65	−2S
e4	0.76	0.80	e5	0.8	0.77	+1D
e5	0.91	0.88	e6	0.86	0.82	+2S
		0.89	e7	0.94	1.02	+2P
e6	1.08	1.16				−2P
h1	−0.50	−0.46	h1	−0.28	−0.26	+1S
h2	−0.65	−0.64	h2	−0.39	−0.39	−1S
		−0.67	h3	−0.44	−0.41	−1P
h3	−0.76	−0.81	h4	−0.54	−0.51	+1P
		−0.84	h5	−0.57	−0.53	+1D
h4	−0.93	−0.96	h6	−0.63	−0.60	−1D
h5	−1.06	−1.02	h7	−0.69	−0.66	+2S
		−1.03	h8	−0.78	−0.81	−2S
			h9	−0.86	−0.83	−2P

$$C_{\text{dot-sub}} = 2\pi\varepsilon_0 r_{\text{dot}}\left[\ln\left(\frac{r_{\text{dot}}}{d_{\text{dot-sub}}}\right) + \ln 2 + \frac{23}{20}\right], \quad (2b)$$

$$\gamma = \frac{1}{1 + \frac{r_{\text{tip}}}{r_{\text{dot}}}}. \quad (2c)$$

Thus, $d_{\text{dot-sub}}$ is determined by a monolayer thickness of tilted dithiol molecules (0.6 nm). The $d_{\text{tip-dot}}$ varied between 0.5 to 2.5 nm, determined by the set-point current that adjusts the approach distance to the CQDs. Considering the mentioned parameters, η was determined to vary between 0.65 to 0.75.

A large value of η (>0.5) reflects a large $C_{\text{dot-sub}}$ value, permitting a larger voltage drop on the tip-dot junction with respect to the drop across the dot-substrate area. Such a situation guarantees a short tunneling rate out of the CQD and a tunneling of one carrier at a time through the CQD (known as a shell tunneling regime). In that case, the conductance resonances refer to individual electronic states, distributed around V_{bias}=0, as shown in Fig. 2. Charge accumulation may occur when the rate of electron (hole) tunneling into a CQD is shorter than the rate out (known as the shell-filling effect), leading to a split appearance of both electron and hole conductance resonances, due to Coulomb repulsion forces and according to the degeneracy of the states. Such a splitting is not pronounced in the conductance spectra shown in Fig. 2, assuming that the thermal instability existing at 20 K did not blur it completely (*vide infra*). Bipolar transport occurs only in rare cases (when $\eta \sim 0.5$), involving simultaneous tunneling of both electrons and holes from both sides of the zero-conductance gap, shrinking the actual conductance band gap, or occasionally appearing as asymmetric distribution of resonances around V_{bias}=0. The obvious experimental evidence shown in Fig. 2 and the values of η suggests the occurrence of a shell-tunneling process and the data were analyzed accordingly (see below).

The zero-conductance gap is related to the electronic energy band gap by the following relation:[28]

$$\eta\Delta V_{\text{bias}} = E_g + 2\Sigma, \quad (3)$$

$$\Sigma \approx \frac{1}{2}\frac{e^2}{r_{\text{dot}}}\left(\frac{1}{\varepsilon_{out}} - \frac{1}{\varepsilon_{in}}\right) + \frac{0.47e^2}{\varepsilon_{in} r_{\text{dot}}}\left(\frac{\varepsilon_{in} - \varepsilon_{out}}{\varepsilon_{in} + \varepsilon_{out}}\right). \quad (4)$$

The Σ term describes an energy polarization, related to a charge image developed at an exterior medium due to a dielectric mismatch between a CQD and the surrounding. The variables ε_{in} and ε_{out} are the static dielectric constant of the CQD, and the surrounding, respectively (ε_{in}=volume weighted average between $\varepsilon_{s(\text{PbS})}$=161 and $\varepsilon_{s(\text{PbSe})}$=227 and ε_{out} corresponds to a dielectric constant of the surrounding ε_{out}=3).[24]

Based on the relation given in Eq. (3), the conductance spectra can be represented by a log plot of dI/dV_{bias} versus E. Illustrative examples are shown in Fig. 3, showing the spectra of a single PbSe/PbS core-shell CQD with (a) $r_{\text{cs}}=3$ nm and (b) $r_{\text{cs}}=4$ nm. These spectra also contain a stick diagram (dashed lines), offering the theoretical estimation of the intraband levels, when a thicker line corresponds to a proximity or to an overlap of a few electronic states. In general, the theory was derived from the core CQD envelope function **s**, using a bulk $\mathbf{k}\cdot\mathbf{p}$ Hamiltonian.[19] Bloch states of the lowest conduction and topmost valence bands with spin degeneracy were included (a four-band Hamiltonian). The off-set was predicted numerically to be 0.09 eV and was also confirmed recently by cyclic voltometry.[29] The form of the Hamiltonian uniquely determined the boundary conditions at the PbSe/PbS interface, adopting a procedure supplied by Burt,[30] when considering the discontinuity in the effective mass as well as in the dielectric constant. Eventually, the Hamiltonian of the core-shell structure showed dependence on radial coordinates only, so, the material's parameters can be characterized by the principal (radial) quantum number n, orbital angular momentum l, and a parity π. Accordingly, Table I summarizes the assignments of the various electronic levels following the notation of $(\pi)(n)(l)$. For example, "+2s" means $\pi=+1$, $n=2$, and $l=0$. Figure 3 reveals a relatively close match between the position of the STS resonance bands and the theoretical electronic levels. However, the experimental resonances have a FWHM between 40–120 meV, with nearly equivalent broadening within the valence and conduction band states. Such a large broadening is beyond expectations for measurements carried out at cryogenic temperatures. It suggests that most of the broadening is not related to a thermal fluctuation. Instead, it is governed by an electron-phonon coupling with a larger influence on the smallest CQD, on fluctuation of charges in the surrounding of the CQD, or displacement of the CQD in the junction.[31] It should be noted that similar resonance full width at half maximum (FWHM) of electrons and holes reflects a symmetric distribution around the Fermi level, as suggested previously in core PbSe CQDs,[1] and it seems to be preserved in the core-shell structures discussed in this paper.

The estimated electronic energy band-gap values, derived by Eqs. (3) and (4), versus a CQD's radius (r_{c} or r_{cs}) are plotted by the black squares in Fig. 4(a). These values are compared with band gap derived from the absorption spectra (blue squares in the figure). The measured absorption gap was corrected for the electon-hole Coulomb interaction generated upon illumination, using the following expression:[32]

$$J_{\text{e-h}}(r_{\text{cs}}) = \frac{e^2}{r_{\text{cs}}}\left(\frac{1}{\varepsilon_{out}} + \frac{0.79}{\varepsilon_{in}}\right). \tag{5}$$

Also, the measured absorption gap at room temperature was extrapolated to its value at 20 K, using the band-edge temperature coefficient $d\alpha/dT$, measured elsewhere.[22] A theoretical estimation of the energy band gap, derived by the effective-mass approximation for the core-shell CQDs studied, is marked by the red squares in the figure while absorption edges of pure PbSe CQDs with similar radii, measured by STS technique (adopted from Ref. 24), are shown by the green circles in Fig. 4(a). The band-gap values, revealed by the different measurements, are also listed in Table II. The figure and the table show that the band-gap energy decreases with the increase in the shell width, a general trend that appeared in the STS and absorption spectra, as well as by the theoretical evaluation. However, the STS measurements deviate by ~20% from those of absorption and theoretical points. This deviation might be related to accumulated errors in the measured values of r_{tip} and $r_{\text{tip-dot}}$. In any event, the change in the energy band gap of the core-shell samples with the increase in the shell width (or total radius of the structure), is moderate with respect to a change that is observed by a simple increase in a PbSe core radius (following the trend of the green circles in Fig. 4). This comparison suggests the spread of the electron and/or wave functions over the entire core-shell structure, however, the change in the effective mass and dielectric constant at the core-shell interface governs different delocalization of the carriers within the core and the shell, causing the electronic nature to be slightly different from a pure PbSe medium of a similar size.

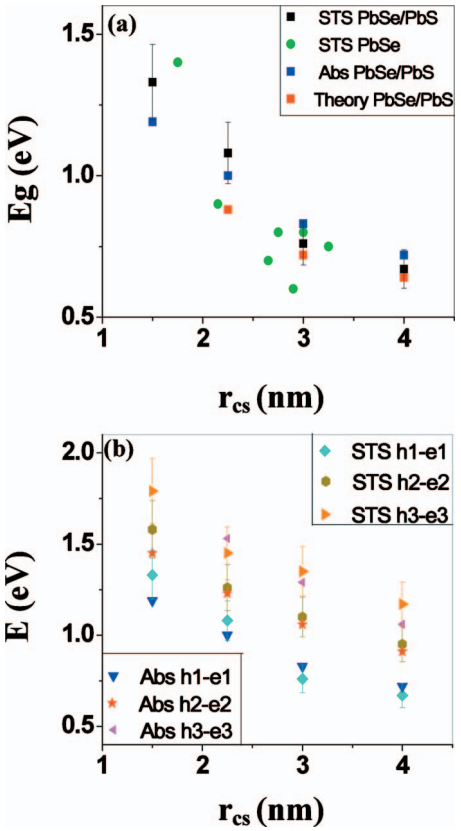

FIG. 4. (Color) (a) A plot of the energy band gap of PbSe or PbSe/PbS structures, versus the CQD's outer radius (r_{cs}), as measured by STS and absorption spectroscopy, or predicted theoretically, following the given symbols in the legend. (b) A plot of a few interband energy transitions versus PbSe or PbSe/PbS CQD's outer radius, as measured by STS and absorption spectroscopy, according to the designation given in the legend.

Figure 4(b) represents a plot of the energy spacing between a few interband levels, h1-e1, h2-e2, and h3-e3 versus the total size of the core-shell CQDs (r_{c} or r_{cs}). The energy of each interband level is actually an average value of proxi-

TABLE II. Experimental values of the energy band gap of PbSe/PbS CQDs of various outer radii (r_{cs}), compared with a theoretical evaluation and with the band-gap energy of PbSe cores of similar radii.

r_{cs} (nm)	E_g (eV)			
	Absorption	STS	Theory	PbSe[a]
1.50	1.19	1.33 ± 0.13		
1.75				1.40
2.15				0.90
2.25	1.00	1.08 ± 0.11	0.88	
2.65				0.70
2.75				0.80
2.90				0.60
3.00	0.83	0.76 ± 0.08	0.72	0.80
3.25				0.75
4.00	0.72	0.67 ± 0.07	0.64	

[a]Experimental STS values reported in Ref. 24.

mate theoretical states (grey sticks in Fig. 3 or assigned states listed in Table I). The relevant interband transitions extracted from the absorption spectra are also shown in Fig. 4(b), following the symbols given in the legend. The results reveal a good agreement between the STS and absorption measurements, both indicating a decrease in the transition energies of the ground state, as well as hot excitons, with the increase in the outer radii of the core-shell CQDs. The decrease in the interband transition energies is related to the increase in carriers delocalization over the entire core-shell structure, leading to reduction in the confinement effect.

V. SUMMARY

This paper presented the conductance spectra, measured by a STS, of a set of PbSe/PbS core-shell samples with a common core radius of 1.5 nm and a PbS shell of a variable width (w) from 0.75 to 2.5 nm. The conductance resonances were correlated with a shell tunneling process (with experimental parameter—η, varying from 0.65 to 0.75). The experiment monitored the individual electronic levels of the conduction (e1, e2,…) and valence (h1, h2,…) bands. The energy band gap of the various samples, derived from the STS measurements, showed close agreement to the values measured by the absorption spectra, as well as with theoretical predictions. The theoretical model was based on an extended four-band envelope function theory across the PbSe/PbS material boundary, including the Fermi-energy offset at the interface and a discontinuity in the effective mass and in the dielectric constant. The experimental and theoretical results showed a decrease in the energy band gap, and of a few other hot interband transitions, with the increase in the shell thickness. This result was correlated with a reduction in the band gap upon delocalization of the carriers' wave functions over the entire core-shell structure, consistent with the previous expectations for PbSe/PbS core-shell CQDs with an outer radii <5 nm.[19] The study supplies information regarding the change in the electronic configuration with the variation in composition and core radius/shell width, indicating particular merit for the application of those near infrared active CQDs with good chemical robustness in solar energy and gain devices.

ACKNOWLEDGMENT

The research was supported by the USA-Israel Binational Science Foundation, Project No. 2006225.

*Corresponding author; meiravsaraf@yahoo.com
†Corresponding author; ssefrat@techunix.technion.ac.il

[1] I. Kang and F. W. Wise, J. Opt. Soc. Am. B **14**, 1632 (1997); F. W. Wise, Acc. Chem. Res. **33**, 773 (2000); S. V. Goupalov, Phys. Rev. B **79**, 233305 (2009).
[2] E. Lifshitz, M. Brumer, A. Kigel, A. Sashchiuk, M. Bashouti, M. Sirota, E. Galun, Z. Burshtein, A. Q. Le Quang, I. Ledoux-Rak, and J. Zyss, J. Phys. Chem. B **110**, 25356 (2006).
[3] G. Allan and C. Delerue, Phys. Rev. B **70**, 245321 (2004); Mater. Sci. Eng., C **25**, 687 (2005).
[4] M. Brumer, M. Sirota, A. Kigel, A. Sashchiuk, E. Galun, Z. Burshtein, and E. Lifshitz, Appl. Opt. **45**, 7488 (2006).
[5] M. Law, J. M. Luther, Q. Song, B. K. Hughes, C. L. Perkins, and A. J. Nozik, J. Am. Chem. Soc. **130**, 5974 (2008).
[6] K. W. Johnston, A. G. Pattantyus-Abraham, J. P. Clifford, S. H. Myrskog, D. D. MacNeil, L. Levina, and E. H. Sargent, Appl. Phys. Lett. **92**, 151115 (2008).
[7] K. P. Fritz, S. Guenes, J. Luther, S. Kumar, N. S. Sariciftci, and G. D. Scholes, J. Photochem. Photobiol., A **39**, 195 (2008).
[8] J. C. Johnson, K. A. Gerth, Q. Song, J. E. Murphy, and A. J. Nozik, Nano Lett. **8**, 1374 (2008).
[9] B. R. Hyun, H. Chen, D. A. Rey, F. W. Wise, and C. A. Batt, J. Phys. Chem. B **111**, 5726 (2007).
[10] L. Etgar, E. Lifshitz, and R. Tannenbaum, J. Phys. Chem. C **111**, 6238 (2007).
[11] C. B. Murray, S. Shouheng, W. Gaschler, H. Doyle, T. A. Betley, and C. R. Kagan, IBM J. Res. Dev. **45**, 47 (2001); A. Sashchiuk, L. Langof, R. Chaim, and E. Lifshitz, J. Cryst. Growth **240**, 431 (2002); B. L. Wehrenberg, C. Wang, and P. Gyuot-Sionnest, J. Phys. Chem. B **106**, 10634 (2002); W. W. Yu, J. C. Falkner, B. S. Shih, and V. L. Colvin, Chem. Mater. **16**, 3318 (2004).
[12] M. Brumer, A. Kigel, L. Amirav, A. Sashchiuk, O. Solomesch, N. Tessler, and E. Lifshitz, Adv. Funct. Mater. **15**, 1111 (2005).
[13] J. M. Pietryga, D. J. Weerder, D. J. Williams, J. L. Casson, R. D. Shaller, V. I. Klimov, and J. A. Hollinsworth, J. Am. Chem. Soc. **130**, 4879 (2008).
[14] R. D. Schaller, M. Sykora, J. M. Petriyga, and V. I. Klimov, Nano Lett. **6**, 424 (2006); J. E. Murphy, M. C. Beard, A. G. Norman, S. P. Ahrenkiev, J. C. Johnson, P. Yu, O. I. Micic, R. J. Ellingson, and A. J. Nozik, J. Am. Chem. Soc. **128**, 3241 (2006); A. Shabaev, Al. L. Efros, and A. J. Nozik, Nano Lett. **6**, 2856 (2006).

[15] R. Osovsky, D. Cheskis, V. Kloper, M. Kroner, A. Sachshuik, and E. Lifshitz, Phys. Rev. Lett. **102**, 197401 (2009).
[16] J. M. An, A. Franceschetti, S. V. Dudiy, and A. Zunger, Nano Lett. **6**, 2728 (2006).
[17] J. M. An, A. Fraceschetti, and A. Zunger, Nano Lett. **7**, 2129 (2007).
[18] R. Koole, G. Allan, C. Delerue, A. Meirjerinc, D. Vanmaekelbergh, and A. J. Houtepen, Small **4**, 127 (2008).
[19] A. C. Bartnik, F. W. Wise, A. Kigel, and E. Lifshitz, Phys. Rev. B **75**, 245424 (2007).
[20] S. H. Wei and A. Zunger, Phys. Rev. B **55**, 13605 (1997).
[21] J. M. Harbold, H. Du, T. D. Krauss, K. S. Cho, C. B. Murray, and F. W. Wise, Phys. Rev. B **72**, 195312 (2005); J. M. Harbold and F. W. Wise, *ibid.* **76**, 125304 (2007).
[22] A. Kigel, M. Brumer, G. I. Maikov, A. Sashchiuk, and E. Lifshitz, Small **5**, 1675 (2009).
[23] E. P. A. M. Bakkers, Z. Henz, A. Zunger, A. Fransachetti, L. P. Kouwenhoven, and D. Vanmakelbergh, Nano Lett. **1**, 551 (2001).
[24] P. Liljeroth, P. A. Zeijlmans van Emmichoven, S. G. Hickey, H. Weller, B. Grandidier, G. Allan, and D. Vanmaekelbergh, Phys. Rev. Lett. **95**, 086801 (2005).
[25] U. Banin, Y. W. Cao, D. Katz, and O. Millo, Nature (London) **400**, 542 (1999); O. Millo, D. Katz, Y. W. Cao, and U. Banin, Phys. Rev. B **61**, 16773 (2000); Phys. Rev. Lett. **86**, 5751 (2001); T. Maltezopoulos, A. Bolz, C. Meyer, C. Heyn, W. Hansen, M. Morgenstern, and R. Wiesendanger, *ibid.* **91**, 196804 (2003).
[26] O. Millo, D. Katz, D. Steiner, E. Rothenberg, T. Mokari, M. Kazes, and U. Banin, Nanotechnology **15**, R1 (2004); O. Millo, D. Steinera, D. Katz, A. Aharonib, S. H. Kanb, T. Mokarib, and U. Banin, Physica E (Amsterdam) **26**, 1 (2005).
[27] D. Steiner, D. Dorfs, U. Banin, F. D. Sala, L. Manna, and O. Millo, Nano Lett. **8**, 2954 (2008).
[28] D. Sarid, *Exploring Scanning Probe Microscopy with Mathematic*, 2nd ed. (Wiley-Interscience, New York, 2006), p. 181; B. Zaknoon, G. Bahir, C. Saguy, R. Edrei, A. Hoffman, R. A. Rao, R. Muralidhar, and K. M. Chang, Nano Lett. **8**, 1689 (2008).
[29] B. R. Hyun, Y. W. Zhong, A. C. Bartnik, L. S. H. D. Abruna, F. W. Wise, J. D. Goodreau, J. R. Matthews, T. M. Lesil, and N. F. Borrelli, ACS Nano **2**, 2206 (2008).
[30] M. G. Burt, J. Phys.: Condens. Matter **11**, 53 (1999).
[31] Z. Sun, I. Swart, C. Delerue, D. Vanmaekelbergh, and P. Liljeroth, Phys. Rev. Lett. **102**, 196401 (2009); L. Jdira, K. Overgaag, R. Stiufiuc, B. Grandidier, C. Delerue, S. Speller, and D. Vanmaekelbergh, Phys. Rev. B **77**, 205308 (2008).
[32] Y. M. Niquet, C. Delerue, G. Allan, and M. Lannoo, Phys. Rev. B **65**, 165334 (2002).